Reconstructed three-dimensional electron momentum density in lithium: A Compton scattering study

Yoshikazu Tanaka

The Institute of Physical and Chemical Research (RIKEN), Mikaduki, Sayo, Hyogo 679-5148, Japan

Y. Sakurai

Japan Synchrotron Radiation Research Institute (JASRI), Mikaduki, Sayo, Hyogo 679-5198, Japan

A. T. Stewart

Physics Department, Queen's University, Kingston, Ontario K7L 3N6, Canada

N. Shiotani

Tokyo University of Fisheries, Kounan 4-5-7, Minato, Tokyo 108-8477, Japan

P. E. Mijnarends

Department of Physics, Northeastern University, Boston, Massachusetts 02115
and Interfaculty Reactor Institute, Delft University of Technology, 2629 JB Delft, The Netherlands

S. Kaprzyk

Academy of Mining and Metallurgy, Cracow, Aleja Mickiewicza 30, Poland
and Department of Physics, Northeastern University, Boston, Massachusetts 02115

A. Bansil

Department of Physics, Northeastern University, Boston, Massachusetts 02115

The three-dimensional electron momentum density $\rho(\mathbf{p})$ in Li is reconstructed via a direct Fourier transform method which is free from functional assumptions concerning the shape of $\rho(\mathbf{p})$. For this purpose, 12 high-resolution Compton profiles are measured, and corresponding highly accurate computations carried out within the band theory framework. Extensive comparisons between the $\rho(\mathbf{p})$'s reconstructed from the theoretical and experimental profiles with each other and with the true (without reconstruction) underlying computed $\rho(\mathbf{p})$ are used to gain insight into the accuracy of our procedures, and to delineate the effects of various parameters (filtering, resolution, etc.) on the reconstructed $\rho(\mathbf{p})$. The propagation of errors is considered in detail, and a general formula appropriate for the present direct Fourier method is derived. The experimental $\rho(\mathbf{p})$ (in comparison to the theoretical results) shows a substantially more smeared out break at the Fermi momentum p_f, and a shift of spectral weight from below to above p_f, clearly indicating the importance of electron correlation effects beyond the local-density approximation for a proper description of the ground-state momentum density. The question of deducing Fermi-surface radii in terms of the position of the inflection point in the slope of $\rho(\mathbf{p})$ in the presence of finite resolution is examined at length. The experimental Fermi surface and its asphericity is in good overall accord with theoretical predictions, except that band theory predicts a bulging of the Fermi surface along the [110] direction, which is greater than seen in the measurements; however, our analysis suggests that the set of 12 directions used in the present experiments may not be optimal (in number or orientations) for observing this rather localized Fermi-surface feature.

I. INTRODUCTION

Properties of the ground state are of fundamental importance for understanding the nature of electronic states and the associated excitation spectrum of materials. Accordingly, as second and third generation synchrotron light sources have come on line in recent years, there has been a resurgence of interest in high-resolution Compton scattering as a direct probe of the electronic ground state.[1–13] The measured Compton profile (CP) $J(p_z)$ is proportional to the twice integrated electron momentum density $\rho(\mathbf{p})$:

$$J(p_z) = \int \int \rho(\mathbf{p}) dp_x dp_y, \quad (1.1)$$

where the z axis lies along the direction of the x-ray scattering vector. Within the independent-particle model, $\rho(\mathbf{p})$ can be expressed as[14]

$$\rho(\mathbf{p}) = (2\pi)^{-3} \sum_{\mathbf{k},\nu}^{\text{occ.}} \left| \int \psi_{\mathbf{k},\nu}(\mathbf{r}) \exp(-i\mathbf{p}\cdot\mathbf{r}) d\mathbf{r} \right|^2, \quad (1.2)$$

where $\psi_{k\nu}(\mathbf{r})$ denotes the electron wave function for state $\mathbf{k}$ and band ν, and the summation is over all occupied states.

Equation (1.2) makes it obvious that in a metallic system the CP will contain fingerprints of the positions and sizes of Fermi-surface-related breaks in the underlying momentum density. However, the presence of the double integral in Eq. (1.1) generally tends to obscure this information. One way to circumvent this problem is to measure CP's along a series of directions, and to use the set of two-dimensional (2D) projections in Eq. (1.1) so obtained, to ''reconstruct'' the 3D function $\rho(\mathbf{p})$. Although such reconstruction procedures possess a long history, much of the existing work was limited to the older (low-momentum resolution) Compton data using γ-ray sources. Paucity of experience in this regard with the high-resolution synchrotron-based Compton data provides a great impetus for undertaking a study such as the present one as a means of getting a handle on the Fermi surface signatures and electron correlation effects in $\rho(\mathbf{p})$.

The first method used to reconstruct the momentum density from CP's or one-dimensional positron annihilation angular correlation spectra[15] was formulated by Mijnarends[16,17] who, in the vein of Cormack's approach,[18] expanded both $\rho(\mathbf{p})$ and the measured profiles into lattice harmonics and derived a relation between the two expansions. Another way to obtain $\rho(\mathbf{p})$ is to utilize the properties of the so-called reciprocal form factor,

$$B(\mathbf{r}) = \int \int \int \rho(\mathbf{p}) \exp(-i\mathbf{p}\cdot\mathbf{r}) d\mathbf{p}. \qquad (1.3)$$

It follows from Eqs. (1.1) and (1.3) that

$$B(0,0,z) = \int_{-\infty}^{\infty} J(p_z) e^{-izp_z} dp_z. \qquad (1.4)$$

If z is chosen along the various scattering vectors, the Fourier transformed CP's yield $B(\mathbf{r})$ along radii in $\mathbf{r}$ space. From there onward one can follow two different approaches to obtain $B(\mathbf{r})$ in all of $\mathbf{r}$ space: Either one expands $B(\mathbf{r})$ into a set of appropriately chosen basis functions,[19] or one straightforwardly maps $B(\mathbf{r})$ in $\mathbf{r}$ space by interpolation. The latter method is called the direct Fourier transform method, and makes no implicit functional assumptions concerning the shape of $\rho(\mathbf{p})$. Once $B(\mathbf{r})$ is known, $\rho(\mathbf{p})$ can then be obtained by Fourier transformation:

$$\rho(\mathbf{p}) = (2\pi)^{-3} \int \int \int B(\mathbf{r}) \exp(i\mathbf{p}\cdot\mathbf{r}) d\mathbf{r}. \qquad (1.5)$$

Hansen[19] applied Eq. (1.4) to obtain the $B(\mathbf{r})$ function, followed by an expansion of $B(\mathbf{r})$ into lattice harmonics. This method is often called the Fourier-Bessel method. Hansen also presented an error analysis. Both Mijnarends' and Hansen's method were computer coded.

The direct Fourier method was first applied to reconstruct the 3D electron-positron momentum density from the 2D angular correlation of positron annihilation radiation measured by Suzuki *et al.* on Ti and Zr.[20] Later, the method was applied to reconstruct the 3D spin-dependent momentum density (i.e., the difference between the majority and minor-

ity spin densities) from magnetic CP's of Fe by Tanaka *et al.*[21,22] In these studies, no corresponding error map was given because a method to analyze the error propagation was not yet developed at the time.[23] Recently, Cormack's method was developed further by Kontrym-Sznajd *et al.*,[24] and applied by Dugdale *et al.*[25] to the reconstruction of the 2D electron momentum density of Cr from several directional CP's. The essential ingredient of Cormack's method is the expansion of both CP's and momentum density into polar Fourier series. Finally, the maximum entropy method, which is already an established method in the field of charge-density reconstruction, was adapted to momentum density reconstruction by Dobrzynski and Holas.[26]

The momentum density and the Fermi surface of bcc Li were repeatedly studied by Compton scattering, because Li upon cooling below about 75 K undergoes a partial Martensitic transformation to a phase which was long believed to be hcp but is now considered to be a $9R$-related samarium-type of structure with numerous stacking faults.[27] It is therefore impossible to apply conventional techniques to measure the Fermi-surface calipers in bcc Li, although a high-magnetic-field study of the de Haas–van Alphen effect in a dispersion of micrometer-sized grains of Li yielded the overall radial distortion.[28]

The first high-resolution, high-statistics measurements of the CP's of Li were reported by Sakurai *et al.*,[4] who deduced the Fermi surface calipers along the three high-symmetry directions by analyzing the second derivatives of the measured profiles. Schülke *et al.*[5] employed the Fourier-Bessel method[19] to reconstruct the momentum density from 11 measured directional profiles, and obtained the corresponding error map. This was the first serious attempt to reconstruct the momentum density in a metal from CP's. Reference 5 also reconstructed the occupation number density to map out the asphericity of the Fermi surface in the (110) plane, and discussed the quasiparticle renormalization parameter Z_k by fitting the occupation number density near the Fermi wave vector on the [100] axis to a jellium model. The value $Z_k = 0.1 \pm 0.1$ deduced in this manner is strikingly smaller than the predictions of a variety of electron-gas calculations stretching over the last several decades, which yielded Z_k values in Li ranging from 0.65 to 0.82.[29–34] It is difficult to explain such a low value of Z_k within the framework of the plasmaron-type physics underlying the conventional picture of the interacting electron gas.[35–39] We note, however, that the analysis of Compton data from a series of LiMg disordered alloys by Stutz *et al.*[11] hinted that the behavior of Li may be idiosyncratic rather than being representative of metals more generally.

Bearing all this in mind, we have been motivated to undertake the present study for several reasons. First, to develop the direct Fourier transform technique further and to analyze in particular the error propagation within this reconstruction procedure. Second, to apply this method to reconstruct the momentum density of a realistic system in order to assess how reconstruction and digital filtering affects the overall resolution. Finally, our choice of Li for this study is a natural one, since Li with its simple electronic structure recently took on the role of touchstone for trying out ap-
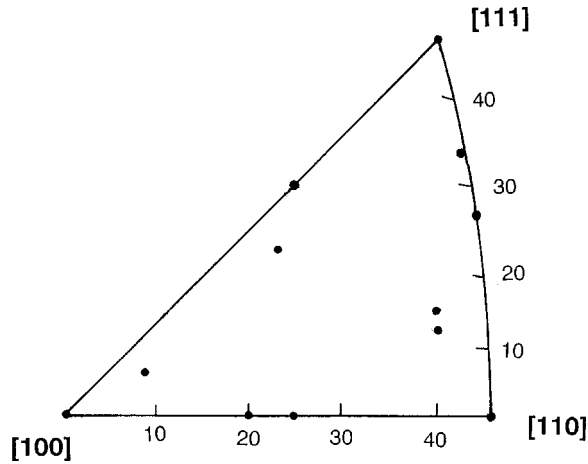
FIG. 1. Stereographic plot of the 12 directions along which the Compton profiles of Li are measured for reconstruction of the three-dimensional momentum density.

proaches involving the Compton spectra. Of course there is also an intrinsic interest in carrying out a reconstruction of the momentum density of Li independent of the earlier work of Ref. 5, and to compare experiment and theory as to the overall shape of the momentum density, the asphericity of the Fermi surface, and related issues. Concerning differences between our work and that of Ref. 5, apart from the use of a different method of reconstruction, a few further points may be noted. We determine the Fermi-surface calipers straightforwardly via the position of the inflection point in the slope of the momentum density, without invoking the secondary assumptions of Ref. 5 related to the reconstructed occupation function. The momentum resolution of our experiments is slightly better, and the effect of resolution on the determination of the Fermi radii is delineated in detail. Despite these differences, it is satisfying to see that there is good overall accord between our results and those of Ref. 5, suggesting that these results are fairly robust.

An outline of this paper is as follows. The introductory remarks are followed in Sec. II with a brief discussion of the experimental procedures. Section III outlines the theoretical methodology. In Sec. IV, relevant details of the direct Fourier method for momentum-density reconstruction are described. Section V presents an analysis of the error propagation. Section VI discusses the experimental and theoretical results concerning the momentum density and Fermi surface of Li. A few concluding remarks are made in Sec. VII. The derivations in the appendixes which tackle some of the technical issues are straightforward but somewhat unfamiliar, and we hope that their inclusion will help the readability of the text.

II. EXPERIMENT

The CP's along 12 crystalline directions indicated in Fig. 1 were measured with the multiarm, high-resolution Compton spectrometer installed at the beamline NE1 of the High Energy Accelerator Research Organization. The details of this spectrometer were described by Sakurai et al.[40] X rays from a multipole wiggler were monochromatized by a quasi-

doubly-bent monochromator[41] to 59.38 keV, with an energy resolution of about 70 eV. The spectrometer has three arms, each possessing a Cauchois-type Si (422) bent-crystal analyzer with an image plate (IP) as a position sensitive detector. These are mounted on the surface of a cone whose axis lies along the path of the incident x rays, so that each arm defines a scattering angle of 160°. The spectrometer thus measures CP's along three different scattering vectors at one time. The Compton-scattered x rays are angle dispersed by the analyzer, and detected via the number of color centers generated in the IP. The image stored on the IP is read by a scanning He-Ne laser beam over a mesh containing 1280 $\times$ 1280 pixels of size 0.1×0.1 mm^2. The details of the read-out system of the IP were described by Amemiya et al.[42] The width between two adjacent channels in the IP corresponds to 0.023, 0.025, and 0.031 a.u. at $p_z = -10$, 0, and 10 a.u. in a CP, respectively.

Single crystals of Li grown by a modified Bridgman technique were cut into five disk-like 4-mm-thick samples with surface normals along the [100], [110], [111], [211], and [221] crystalline directions, respectively. The crystals were etched and cleaned by pure ethanol. The sample was mounted on a small goniometer, and set in a vacuum chamber which was evacuated to less than 10^{-7} torr. Typical accumulated counts in one channel at the Compton peak are 2.4×10^5. Multiple-scattering events were simulated using a Monte Carlo method computer coded by Sakai.[43] The fraction of multiple-scattering events was found to be about 3.6% of the single Compton scattering events in all cases. The background noise was determined in the same way as described in Ref. 4.

The [100], [110], and [111] CP's are the same as those presented previously by Sakurai et al.[4] We note, however, that we have subtracted the computed solid-state core profiles to obtain the valence CP's. The overall momentum resolution is 0.12 a.u. at $p_z = 0$. The standard deviations (error bars) were evaluated as follows. The data stored in the IP contain errors originating in the photon counting process, in addition to errors introduced by the read-out system. These errors depend mainly on the stability of the laser and the uniformity of the photostimulable phosphor in the IP. The nonuniformity of the total IP response has been estimated to be about 0.5 % by Ito et al.;[44] the total standard deviation σ for N counts is given by

$$\sigma = \sqrt{N} + 0.005 \times N. \qquad (2.1)$$

As a typical example, the value of σ at the peak of the CP along the [100] axis is about 0.7% of N.

III. COMPTON PROFILE COMPUTATIONS

The calculations use the all electron charge self-consistent Korringa-Kohn-Restoken band-structure scheme; the crystal potential is based on the von Barth–Hedin local-density approximation to the exchange-correlation functional, and possesses a muffin-tin form.[45–48] The band-structure problem was solved to a high degree of self-consistency (energy bands, Fermi energy, and crystal potential converged to about 1 meV) for the bcc Li lattice ($a = 6.6163$ a.u.) before

proceeding with the CP calculations.[49] The Lam-Platzman correction to the CP's was obtained using the occupation number density for the uniform electron gas.[50] For the CP computations, the momentum density was evaluated on a mesh with 87265×177 **p** points extending to about 5.0 a.u. This mesh corresponds to 87265 *ab initio* **k** points in the irreducible 1/48th of the Brillouin zone, with each **k** point translated to obtain 177 **p** points using reciprocal-lattice vectors. In order to compute the CP's efficiently, a vectorized version of the linear tetrahedron method in which one zooms in on the momentum region in the vicinity of the Fermi surface breaks (with a concomitant increase in the effective density of **p** points) was used. The CP's of Li presented here involve no essential approximation beyond the basic local-density approximations, (LDA); various other approximations, such as the muffin-tin form of the potential, are believed not to be significant. The final CP's were computed over a momentum mesh of 0.001 a.u. and are accurate to a few parts in 10^4.

IV. RECONSTRUCTION

Equation (1.4) shows that the Fourier transform of a CP gives the values of $B(\mathbf{r})$ along the direction of the scattering vector (i.e., the z axis); henceforth we refer to this quantity as a directional $B(r)$. The 12 measured CP's then yield values of B along 12 such rays. Note that the value of $B(0)$ in each case equals the total number of electrons per atom. Using these directional $B(r)$'s, we map out the values of $B(\mathbf{r})$ on a cubic mesh of **r** points by interpolation. An inverse Fourier transform of $B(\mathbf{r})$ then gives the full 3D momentum density $\rho(\mathbf{p})$.

The specific details of the procedure outlined above, relevant for developing the error propagation analysis in Sec. V below, are as follows. Since the mesh over which the CP's are measured is not equidistant, we first interpolate the CP's onto a uniform p_z scale ($\Delta p_z = 0.02$ a.u.) in order to carry out the Fourier transform. The CP's are folded with respect to the origin, $p_z = 0$, which reduces the error bars. The CP's over the range from 0 to 4 a.u. are written as $J_l(k\Delta p)$, where $0 \leq k \leq 200$ is an integer, $\Delta p = 0.02$ a.u., and $l = 1, 2, \ldots, 12$ is a directional index. Then the directional B's may be expressed as

$$B_l(j\Delta r) = 2\Delta p \sum_{k=0}^{n}{}' J_l(k\Delta p)\cos\left(jk\frac{2\pi}{N}\right),$$

$$j = 0, 1, 2, \ldots, n, \tag{4.1}$$

and, conversely, the J's are expressed as

$$J_l(k\Delta p) = \frac{\Delta r}{\pi} \sum_{j=0}^{n}{}' B_l(j\Delta r)\cos\left(jk\frac{2\pi}{N}\right),$$

$$k = 0, 1, 2, \ldots, n. \tag{4.2}$$

Here $\Delta r = 2\pi/(N\Delta p) = 0.153$ a.u., $n = 1024$, $N = 2n$, and Σ' denotes a sum which includes all terms as shown, except that the first and the last term are multiplied by 1/2. We

extend $J(p)$ to 20.48 a.u., and set $J(k\Delta p) = 0$ for $201 \leq k \leq 1024$ to make Δr small enough to describe the $B(r)$ function properly. The factor of 2 in Eq. (4.1) comes from the folding around $p = 0$ noted above. The maximum value of r is $\pi/\Delta p = 157$ a.u.

To reduce high-frequency noise originating from the IP reading process, all the directional $B(r)$'s are multiplied by an empirical filter function,

$$f(r) = \begin{cases} 1 & \text{for } 0 \leq r < 2r_h \\ \frac{1}{2}\left[(r-2r_h)/r_h\right]^2 & \text{for } r \geq 2r_h. \end{cases} \tag{4.3}$$

We use $r_h = 23.1$ a.u. which, as discussed in Appendix A, is consistent with the experimental momentum resolution. After filtering, the values of $B(r)$ for the region $r \geq 2.0 r_h$ become almost comparable to the value of the standard deviation $\sigma[B(r)]$.

Next, we create a simple cubic mesh for $B(\mathbf{r})$ with $257 \times 257 \times 257$ **r** points given by $\mathbf{r} = (2j_x\Delta r, 2j_y\Delta r, 2j_z\Delta r)$, where $j_x, j_y, j_z = 0, 1, \ldots, 256$, and $2\Delta r$ is the distance between adjacent points. The value of $B(\mathbf{r})$ at each **r** point is obtained by interpolation as follows. The 12 $B(r)$ functions are first represented via third-order polynomials with coefficients determined by a spline fit, so that the value of $B(r)$ can be obtained for an arbitrary value of r. The value of $B(\mathbf{r})$ is now interpolated as

$$B(j_x, j_y, j_z) = u_1 B_l(r) + u_2 B_m(r) + u_3 B_n(r)$$

$$\text{for} \quad 1 \leq l, m, n \leq 12. \tag{4.4}$$

Here $r = 2\Delta r\sqrt{(j_x^2) + (j_y^2) + (j_z^2)}$, and B_l, B_m, and B_n are three directional $B(\mathbf{r})$'s whose directions are closest to and enclose the direction (j_x, j_y, j_z). The weights u_1, u_2, and u_3, with $u_1 + u_2 + u_3 = 1$, are proportional to the spherical areas of the triangles made up by these four directions, as outlined in Appendix B.

For $\rho(\mathbf{p})$, we similarly create a simple cubic mesh with $257 \times 257 \times 257$ **p** points given by $\mathbf{p} = (k_x\Delta p/2, k_y\Delta p/2, k_z\Delta p/2)$, where $\Delta p/2 = 0.01$ a.u., and k_x, k_y, and k_z are integers ranging from 0 to 256. The momentum density at **p** is then given by

$$\rho(k_x, k_y, k_z) = \left(\frac{2\Delta r}{\pi}\right)^3 \sum_{j_x=0}^{n}{}' \sum_{j_y=0}^{n}{}' \sum_{j_z=0}^{n}{}' B(j_x, j_y, j_z)$$

$$\times \cos\left[(k_x j_x + k_y j_y + k_z j_z)\frac{2\pi}{N}\right]. \tag{4.5}$$

We set $B(j_x, j_y, j_z) = 0$ for $j_x \geq 257$ or $j_y \geq 257$ or $j_z \geq 257$. Note that the momentum density ρ has the proper dimension of number of electrons per a.u.^{3}

V. PROPAGATION OF ERRORS

An analysis of error propagation requires the evaluation of variances and covariances of various physical variables appearing in the reconstruction process; see Barlowi[51] for a summary of relevant basic relationships. We proceed in the following steps. First, we calculate the variance $\sigma^2[J'(p)]$

of the observed (not-normalized) profile, $J'(p)$, and determine how it is transferred to the variance, $\sigma^2[B'(r)]$, of the corresponding not-normalized B function, $B'(r)$, and the covariance between two points of $B'(r)$. Next we consider the variance and the covariance of the normalized $B(r)$, followed by the variance and covariance of the interpolated $B(\mathbf{r})$. Finally, we obtain the variance of $\rho(\mathbf{p})$.

The standard deviation σ for the experimental (not-normalized) Compton profile J' is given by Eq. (2.1). After folding with respect to $p_z=0$, the variances are

$$\sigma^2[J'(k\Delta p)]=(\sqrt{N_k}+0.005N_k)^2+(\sqrt{N_{-k}}+0.005N_{-k})^2,$$

$$0\leqslant k\leqslant 200. \qquad (5.1)$$

Taking into account the effect of interpolating $J(p_z)$ to an equidistant mesh, the variance propagation in the process of Fourier transforming J' can be expressed as

$$\sigma^2[B'(j\Delta r)]=(\Delta p)^2\sum_{k_1=0}^{n}{}'\sum_{k_2=0}^{n}{}'\cos\left(jk_1\frac{2\pi}{N}\right)$$

$$\times\cos\left(jk_2\frac{2\pi}{N}\right)\mathrm{cov}[J'(k_1\Delta p),J'(k_2\Delta p)],$$

$$(5.2)$$

where $|k_1-k_2|\leqslant 1$ because only adjacent points in $J(k\Delta p)$ are correlated in the process of interpolation to the equidistant mesh; the factor 2 which appears in Eq. (4.1) was already included in Eq. (5.1). The covariance, $\mathrm{cov}[J'(k_1\Delta p),J'(k_2\Delta p)]$, is equal to the variance $\sigma^2[J'(k_1\Delta p)]$ when $k_1=k_2$, and is equal to $bc\,\sigma^2[J'(p_1)]$ when $k_1=k_2\pm 1$; here, in the interpolation process, it is assumed that $J'(k_1\Delta p)=aJ'(p_0)+bJ'(p_1)$, $J'(k_2\Delta p)=cJ'(p_1)+dJ'(p_2)$, and $p_0\leqslant k_1\Delta p\leqslant p_1\leqslant k_2\Delta p\leqslant p_2$.

The covariance of $B'(j_1\Delta r)$ and $B'(j_2\Delta r)$ is given by

$$\mathrm{cov}[B'(j_1\Delta r),B'(j_2\Delta r)]$$

$$=(\Delta p)^2\sum_{k_1=0}^{n}{}'\sum_{k_2=0}^{n}{}'\cos\left(j_1k_1\frac{2\pi}{N}\right)\cos\left(j_2k_2\frac{2\pi}{N}\right)$$

$$\times\mathrm{cov}[J'(k_1\Delta p),J'(k_2\Delta p)], \qquad (5.3)$$

where j_1 and j_2 run from 0 to n, and $|k_1-k_2|\leqslant 1$.

Recalling that $B(0)$ gives the number of valence electrons, we normalize $B'(j\Delta r)$ via

$$B(j\Delta r)=\frac{B(0)}{B'(0)}B'(j\Delta r). \qquad (5.4)$$

The errors in B' are transferred to B through Eq. (5.4). The variance of the normalized $B(j\Delta r)$ is (omitting Δr for convenience)

$$\frac{\sigma^2[B(j)]}{B(0)^2}=\sigma^2\left(\frac{B'(j)}{B'(0)}\right)=\frac{\sigma^2[B'(j)]}{B'(0)^2}+\frac{B'(j)^2}{B'(0)^4}\sigma^2[B'(0)]$$

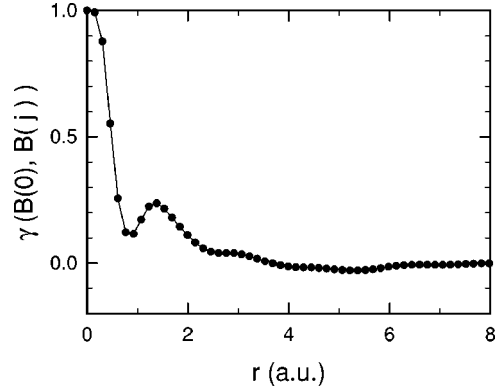$$-\frac{2B'(j)}{B'(0)^3}\mathrm{cov}[B'(0),B'(j)]. \qquad (5.5)$$

FIG. 2. The correlation coefficient $\gamma[B(0),B(j_1)]$ of $B(\mathbf{r})$ on the [100] axis.

Note that $\sigma^2[B(0)]=0$ because the value of the number of the valence electrons is a constant.

The covariance of $B(j_1\Delta r)$ and $B(j_2\Delta r)$ is obtained from Eq. (5.4) as

$$\frac{1}{B(0)^2}\mathrm{cov}[B(j_1),B(j_2)]$$

$$=\frac{1}{B'(0)^2}\mathrm{cov}[B'(j_1),B'(j_2)]$$

$$-\frac{B'(j_1)}{B'(0)^3}\mathrm{cov}[B'(0),B'(j_2)]$$

$$-\frac{B'(j_2)}{B'(0)^3}\mathrm{cov}[B'(j_1),B'(0)]$$

$$+\frac{B'(j_1)B'(j_2)}{B'(0)^4}\sigma^2[B'(0)]. \qquad (5.6)$$

The related correlation coefficient between two points is

$$\gamma[B(j_1),B(j_2)]=\frac{\mathrm{cov}[B(j_1),B(j_2)]}{\sigma[B(j_1)]\sigma[B(j_2)]}. \qquad (5.7)$$

Figure 2 shows a plot of $\gamma[B(0),B(j_1)]$ on the [100] axis, and is illustrative of the shape of the correlation function. Note that this correlation coefficient decreases rapidly, and is large only in a limited region.

We now consider the variance and the covariance of the interpolated $B(\mathbf{r})$. Because each directional $B(\mathbf{r})$ is expanded into a set of third-order polynomials by the spline interpolation, the variance of $B(\mathbf{r})$ at an arbitrary $\mathbf{r}$ is given by the polynomials whose coefficients are squared. Since $B(j_x,j_y,j_z)$ is given in Eq. (4.4), the variance is expressed using $\mathbf{j}=(j_x,j_y,j_z)$ as

$$\sigma^2[B(\mathbf{j})]=u_1^2\sigma^2[B_{l_1}(r)]+u_2^2\sigma^2[B_{l_2}(r)]+u_3^2\sigma^2[B_{l_3}(r)]. \qquad (5.8)$$

Here the covariance between two $B(\mathbf{r})$ functions is zero, because the measurements along two different directions are independent.

The covariance of two points in $B(\mathbf{r})$ is

$$\mathrm{cov}[B(\mathbf{j}_1),B(\mathbf{j}_2)]=\sum_{i}^{3}\sum_{j}^{3}\mathrm{cov}[u_iB_{l_i}(r),u_jB_{l_j}(r)]\delta_{l_i,l_j},\tag{5.9}$$

where the u_i's are the coefficients used in Eq. (4.4), the l_i's are directional indices, and the presence of δ_{l_i,l_j} insures that there is no correlation between B_{l_i} and B_{l_j} when $l_i\neq l_j$.

Finally, the variance of $\rho(\mathbf{p})$ becomes

$$\sigma^2[\rho(\mathbf{k})]=\left(\frac{2\Delta r}{\pi}\right)^6\sum_{\mathbf{j}_1=0}^{\mathbf{n}}{}'\sum_{\mathbf{j}_2=0}^{\mathbf{n}}{}'\mathrm{cov}[B(\mathbf{j}_1),B(\mathbf{j}_2)]$$

$$\times\cos\left[(\mathbf{k}\cdot\mathbf{j}_1)\frac{2\pi}{N}\right]\cos\left[(\mathbf{k}\cdot\mathbf{j}_2)\frac{2\pi}{N}\right],\tag{5.10}$$

where, as before, $\mathbf{k}=(k_x,k_y,k_z)$ is the vector of integers related to the components of $\mathbf{p}$, and $\mathbf{j}=(j_x,j_y,j_z)$. In this equation, $\mathrm{cov}[B(\mathbf{j}_1),B(\mathbf{j}_2)]=\sigma^2[B(\mathbf{j})]$ when $\mathbf{j}_1=\mathbf{j}_2$.

VI. RESULTS AND DISCUSSION

It is important first to assess how well the direct Fourier transform method works under conditions used to reconstruct the experimental momentum density. For this purpose, we apply the method to 12 *theoretical* CP's along directions which are identical to those of the measured profiles (see Sec. III above) and where the answer (i.e., the underlying 3D momentum density) is known independently. The meshes for $B(\mathbf{r})$ and $\rho(\mathbf{p})$ are also chosen to be the same as those used for reconstructing the experimental data. To keep matters relatively simple, the experimental resolution and statistical noise in the data are not included in the theoretical CP's. The reconstruction was carried out with and without the use of the filter function of Eq. (4.3). Figure 3 compares the original $\rho(\mathbf{p})$ and the reconstructed one along three high-symmetry lines. The true $\rho(\mathbf{p})$ (dotted line) possesses a break at the Fermi momentum p_f, and along the [110] direction, a step-wise rise at 0.73 a.u. due to a high momentum component (HMC). In the reconstructed $\rho(\mathbf{p})$, even without the filter (dashed line), the step at p_f is smeared; the smearing of the HMC related step along the [110] direction is comparable (keeping the step size in mind). Our analysis indicates that the reconstruction process effectively introduces a smearing of the Fermi steps which can be viewed as a convolution with a Gaussian of full width at half maximum (FWHM) of 0.03 a.u. The reconstruction also introduces unwanted ripples arising from the sharp variation at p_f in the CP's.

As expected, the inclusion of the low-pass filter in the reconstruction process is seen by comparing solid and dashed curves in Fig. 3 to cause a reduction in the high-frequency oscillations at the expense of introducing greater smoothing. Around p_f, the effective broadening in the filtered case is equivalent to a convolution with a Gaussian with a FWHM of 0.07 a.u., although the filter hardly degrades the step in the HMC along the [110] direction. The size of the break at p_f in the true $\rho(\mathbf{p})$ is significantly smaller along the [110] direction than along the [100] direction due
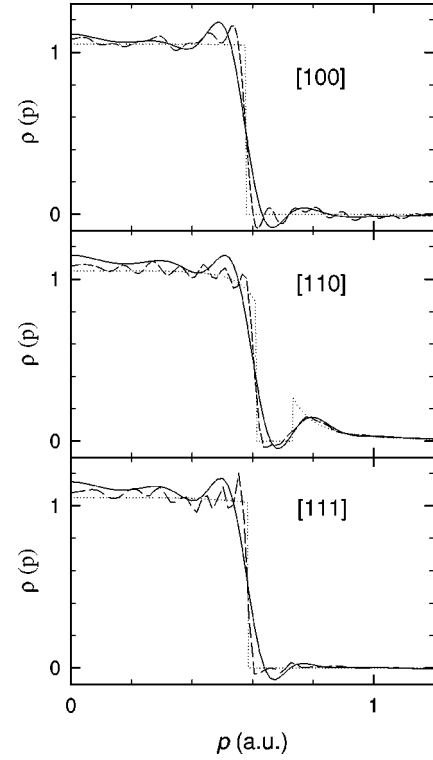

FIG. 3. Comparison of the theoretical $\rho(\mathbf{p})$ along [100], [110], and [111] directions with and without reconstruction. Dotted lines: momentum density computed directly (i.e., without reconstruction). Solid lines: $\rho(\mathbf{p})$ reconstructed from 12 theoretical profiles using the same filter function as that used in reconstructing the experimental profiles. Dashed lines: theoretical $\rho(\mathbf{p})$ reconstructed without the filter function.

to crystal potential effects, but this is not clear in the reconstructed $\rho(\mathbf{p})$, especially when the filter is used. The HMC along the [110] direction in the reconstructed $\rho(\mathbf{p})$'s (with or without filter) is only somewhat ($\sim 60\%$) more pronounced than a similar bump along the [100] or [111] direction and the HMC amplitude is comparable to the size of the spurious ripples around p_f. The value of the reconstructed momentum density is systematically higher than theory at low momenta. Finally, we note that the position of the inflection point in the slope of the reconstructed $\rho(\mathbf{p})$ is systematically found to be lower than the corresponding true p_f values; we shall return to discuss this point later in this section. The preceding remarks should be kept in mind when deducing physical parameters from the reconstructed $\rho(\mathbf{p})$, even though, in view of Fig. 3, the present direct Fourier method works reasonably well overall.

With this background, we compare the $\rho(\mathbf{p})$ reconstructed from the 12 measured CP's with that reconstructed from the 12 corresponding theoretical CP's after the latter are convoluted with the experimental resolution function. Figures 4(a) and 4(b) show the contour maps of the theoretical and experimental $\rho(\mathbf{p})$ in the (110) plane, respectively. Here, the effective total momentum resolution is 0.139 a.u., which is obtained by summing the squares of the instrumental resolution (0.12 a.u.) and the broadening due to reconstruction and filtering (0.07 a.u.). By looking at the density of the contour
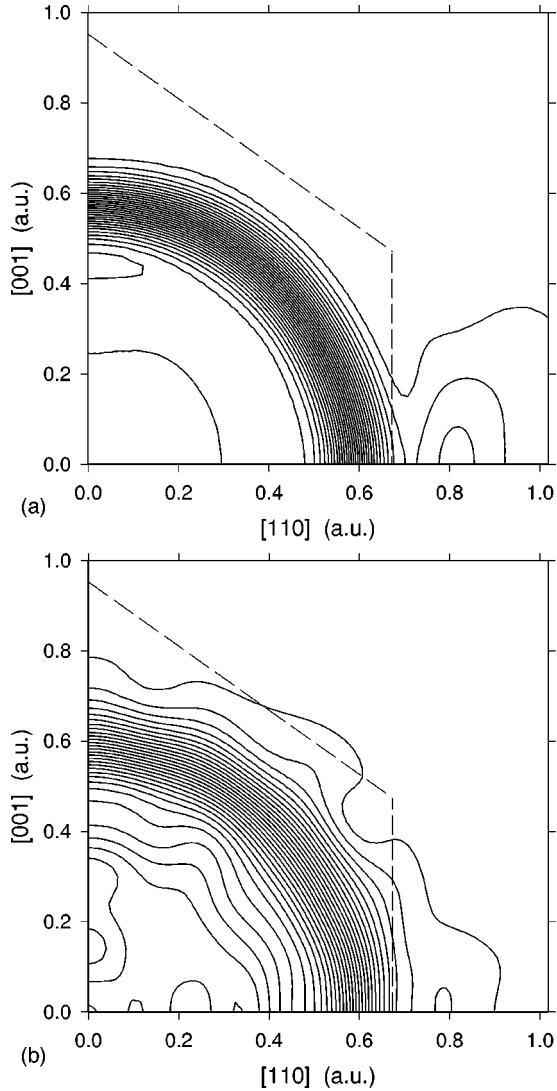
(a)

(b)

FIG. 4. Contour maps of the theoretical (a) and experimental (b) $\rho(\mathbf{p})$ on the (110) plane reconstructed using the filter function. Resolution broadening is included in the theory. The contour interval is 0.035 electrons/a.u.^{3} The dashed lines mark the first Brillouin-zone boundary.

lines it is clear that the experimental break at p_f is broader than predicted theoretically. The HMC-related bump around 0.8 a.u. along the [110] direction is quite distinct in the theory. The signature of this HMC in the experimental data, however, is blurred and barely visible.

Figure 5 shows the error map for the experimental $\rho(\mathbf{p})$. The largest error, 4.1%, is found at $p=0$. Since $\rho(0)=\int B(\mathbf{r})d\mathbf{r}$, the error in $\rho(0)$ is given by the error in the total volume of the $B(\mathbf{r})$ distribution. It is therefore finite, in contrast to the case[17] where $\rho(0)$ is found from $\rho(0)=-(2\pi p)^{-1}(dJ/dp)|_{p=0}$. Although the present reconstruction process involves the entire profile, the fundamental fact remains that the planar integration geometry is unfavorable for obtaining the density at isolated points such as $p=0$. Moving out from $p=0$ along the directions of high symmetry, there is first a rapid decrease of the error, followed by a plateau between $p\sim0.10$ and 0.30 a.u. in the [001] direction,
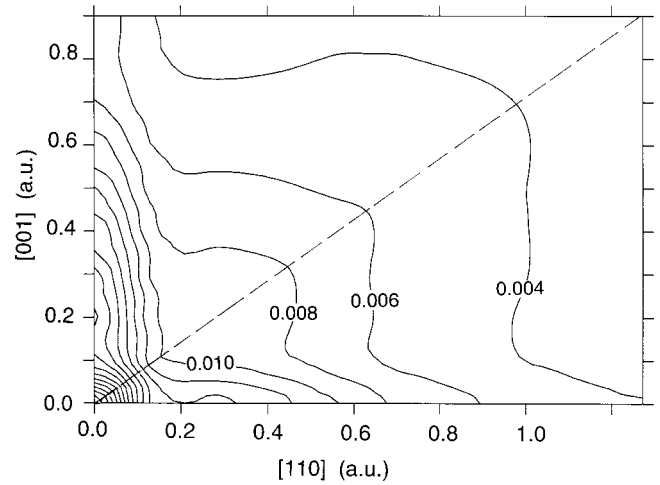

FIG. 5. Contour map of the experimental error bars corresponding to the reconstructed $\rho(\mathbf{p})$ shown in Fig. 4(b). The contour interval is 0.002 electrons/a.u.^{3}

and between $p\sim0.15$ and 0.35 a.u. along the [110] direction where the error does not change much with p. (This is also seen in Fig. 6 where the lengths of the error bars do not seem to change much between $p=0.1$ and 0.4 a.u.) From about 0.4 a.u. onward the error decreases slowly with increasing p and
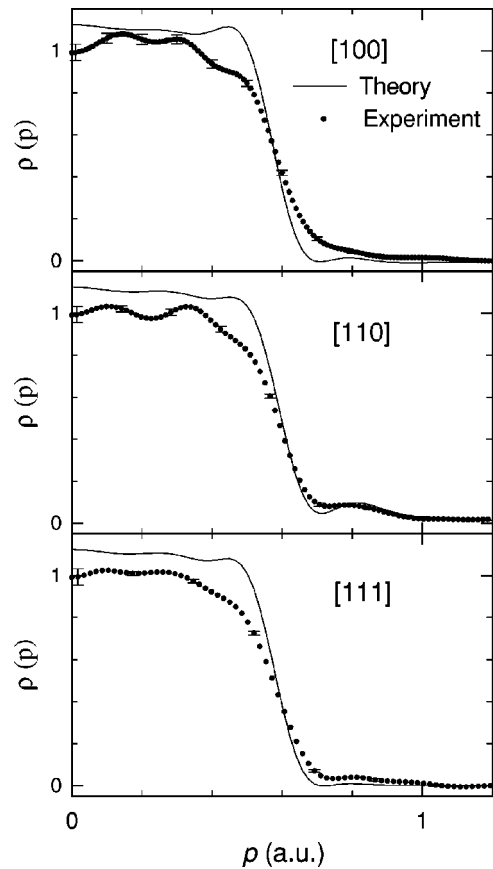

FIG. 6. [100], [110], and [111] sections through the reconstructed theoretical (solid lines) and experimental (dots) momentum densities shown in Fig. 4. Both sets of densities have been normalized such that $B(0)$ equals the number of valence electrons.

it is striking that, for a given p (limiting ourselves to high-symmetry directions), the error bars are generally the largest along the [100] direction, and smallest along the [111] direction, with the [110] direction lying in between. This is due to the terms in Eq. (5.10) with $\mathbf{j}_1 \neq \mathbf{j}_2$, which are proportional to the correlation between two points in $B(\mathbf{r})$, interfering constructively in some directions and destructively in others, giving rise to an uneven accumulation of errors. We emphasize that the asphericity of the error map depends strongly on the crystallographic symmetry. Hansen *et al.*[52] showed that the error may be reduced somewhat (particularly in the [100] direction) if the statistics is increased for high-symmetry profiles in proportion to the statistical weight of the direction. However, even then the error distribution remains strongly anisotropic.

Figure 6 shows sections along the [100], [110], and [111] axes through the reconstructed experimental and theoretical $\rho(\mathbf{p})$'s of Fig. 4. The wiggles in the $\rho(\mathbf{p})$'s are computational artifacts associated with the Fourier transform that cannot be filtered out by the filtering function. In each of these directions, the experimental $\rho(\mathbf{p})$ is seen to lie below theory at low momenta. The situation reverses itself at high momenta, with a crossover point around p_f, where the theoretical slope is distinctly greater (in absolute value) than experiment. Consistent with several recent studies,[4–12] these discrepancies between theory and experiment reflect the effects of electron correlations (beyond the present LDA theory) which shift spectral weight from below to above the Fermi momentum and reduce the size of the break Z_k at the Fermi momentum.[53,54] Reference 5 adduced a nearly zero value of Z_k in Li from an analysis of their CP data. Although our conclusions in this regard are qualitatively similar to those of Ref. 5 (i.e., the measured Z_k is significantly smaller in Li than LDA predictions), we find it difficult to ascribe a definite value to Z_k in view of uncertainties inherent in the reconstructed $\rho(\mathbf{p})$.

We now address the issue of obtaining Fermi surface radii from the structure in $\rho(\mathbf{p})$, and delineate the associated subtleties. The Fermi momentum may be defined straightforwardly as the position of the inflection point given by the minimum in the slope (or equivalently the zero of the second derivative) of $\rho(\mathbf{p})$. In order to gain insight into the accuracy of this procedure, we have carried out a number of simulations. A spherical distribution was simulated first by taking 12 identical profiles each given by the nonconvoluted [100] profile with a Fermi cutoff at 0.5764 a.u. An examination of inflection points along various directions in $\rho(\mathbf{p})$ reconstructed with filtering yielded a spherical Fermi surface of radius 0.5779 a.u., in good agreement with the original value.[55]

The aspherical Fermi surface of Li is considered via two simulations referred to as theory WR and theory NR. Both are based on the filtered reconstruction of the momentum density from the 12 theoretical CP's. The only difference is that in theory WR the experimental resolution is folded in while in theory NR it is not. The theoretical cross section of the Fermi surface in the [110] plane obtained by searching for the inflection points along various directions is compared with the corresponding experimental results in Fig. 7, and a
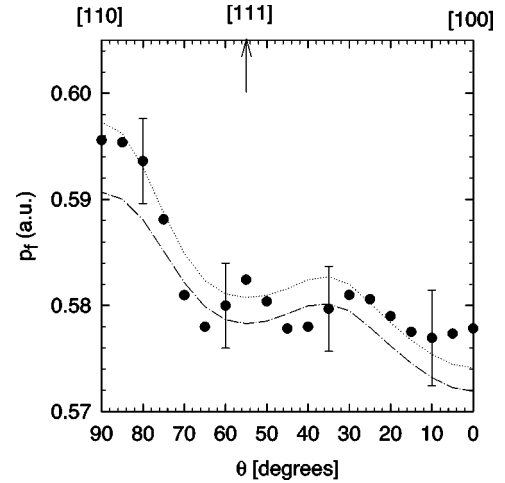

FIG. 7. Uncorrected (see text) Fermi radii in the [110] plane in Li. Theory WR (chain line) and theory NR (dotted line) give results obtained by locating the inflection point in the slope of the $\rho(\mathbf{p})$ reconstructed from 12 filtered theoretical profiles, except that theory WR includes experimental resolution while theory NR does not. The filled circles give (uncorrected) results based on the 12 present experimental profiles.

good overall accord is seen. However this figure does not provide an accurate picture as hinted by the fact that in Fig. 7 theory WR is systematically lower than theory NR. In this connection, Appendix C shows that when the inflection point is used to determine the radius, the effective resolution resulting from the combination of optical resolution, filtering, and reconstruction causes the radius to be *underestimated*. The approximate, model-dependent expression [Eq. (C7)] derived in Appendix C may be used to make a suitable correction.

Figure 8 presents theoretical and experimental radii corrected via Eq. (C7) using appropriate parameters. Accordingly, the corrected theory WR and theory NR radii of Fig. 8 are larger (in relation to the uncorrected values in Fig. 7) by 1% and 0.25%, respectively. A comparison of Figs. 7 and 8 shows that the correction indeed brings the results of theories WR and NR closer to each other, although some residual discrepancies remain, emphasizing the approximate nature of the analysis of Appendix C. The experimental radii were similarly corrected by increasing the values in Fig. 7 by 1% to account for the effective total resolution of 0.139 a.u. Figure 8 also shows the experimental (Compton) results of Schülke *et al.*[5] as well as those obtained by Oberli *et al.*[56,57] from 2D angular correlation of positron-annihilation radiation measurements. It is satisfying to see that within the limitations of the experimental error bars there is a good level of agreement between the three sets of independent experimental points in Fig. 8.

In Fig. 8 we also show (diamonds) the Fermi radii along the three high-symmetry directions obtained directly via band computations without the use of any reconstruction. The [111] and [100] radii are seen to be in reasonably good agreement with the theoretical and experimental values, but the computed [110] radius is distinctly larger than all other reconstructed values. The fact that the reconstructed theoret-
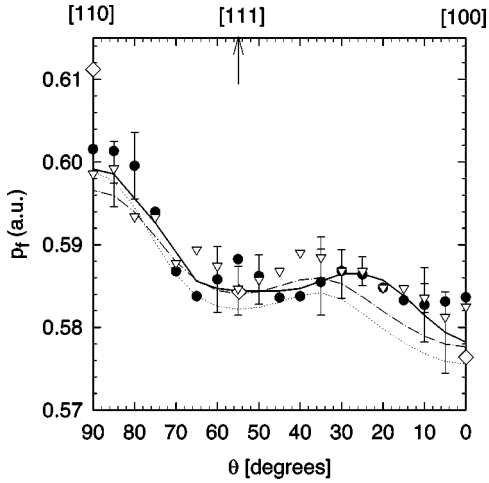
FIG. 8. Corrected (see text) Fermi radii in the [110] plane in Li. Theory WR (chain), theory NR (dots), and present experiments (filled circles) are the same as in Fig. 7, except that the correction based on Eq. (C7) of Appendix C discussed in the text was applied. The open diamonds give the radii along the three principal symmetry directions via band theory computations which do not involve a reconstruction. Earlier results of Refs. 5 (solid line) and 56 (open traingles) are shown for comparison.

ical [110] radius is significantly smaller[58] than its true value (0.6112 a.u.) indicates that the reconstruction is unable to reproduce faithfully the rather local protrusion of the Fermi surface in the [110] direction. This suggests that the present set of 12 directional CP's is not adequate for this purpose, and that to reproduce this feature more directions should be chosen around the [110] axis.

VII. SUMMARY AND CONCLUSION

We have reconstructed the 3D electron momentum density $\rho(\mathbf{p})$ in Li via a direct Fourier transform method which is free from functional assumptions concerning the shape of $\rho(\mathbf{p})$. For this purpose, high-resolution Compton profiles (CP's) have been measured along a set of 12 directions, and highly accurate computations of $\rho(\mathbf{p})$ as well as the CP's along the same set of directions have been carried out within the band theory framework. Extensive comparisons between $\rho(\mathbf{p})$ reconstructed from theoretical CP's with the true (without reconstruction) theoretically computed $\rho(\mathbf{p})$ give insight into the accuracy of our reconstruction procedure, and into how various parameters affect the reconstructed $\rho(\mathbf{p})$. In this way, we show that our method reproduces the structure in the underlying $\rho(\mathbf{p})$ reasonably faithfully, some discrepancies notwithstanding. The reconstruction process itself is shown to yield an effective broadening in $\rho(\mathbf{p})$ of 0.03 a.u (FWHM). The use of a low-pass filter reduces noise at the cost of inducing a further broadening of 0.063 a.u. When combined with our resolution of 0.12 a.u. in the measured CP's, these results imply that the total effective resolution in our filtered reconstructed experimental $\rho(\mathbf{p})$ is 0.139 a.u. The propagation of errors is considered in detail, and an appropriate formula for the present direct Fourier method is derived and applied to the case of our experiments. This

analysis indicates that errors in the reconstructed $\rho(\mathbf{p})$ accumulate unevenly along high-symmetry directions, and that in order to obtain a more uniform distribution of errors a higher statistics along such directions is required. The experimental $\rho(\mathbf{p})$ (in comparison to the corresponding theoretical results) shows a substantially more smeared out break at the Fermi momentum p_f, and a shift of spectral weight from below to above p_f, clearly indicating the importance of including electron correlation effects beyond the LDA for a proper description of the momentum density. The question of adducing the Fermi-surface radius along a given direction from the position of the inflection point in the slope of $\rho(\mathbf{p})$ is examined at length, and it is found that in the presence of a finite resolution such a procedure systematically underestimates the radius; an approximate formula to correct for this error is presented. The Fermi-surface calipers and the anisotropy of the Fermi surface deduced from the reconstructed experimental $\rho(\mathbf{p})$ are in good accord with the corresponding theoretical results as well as with the earlier results in Li based on Compton and positron-annihilation measurements. Notably, however, the band theory predicts a bulging of the Fermi surface along the [110] direction, which is larger than seen in the measurements. In this connection, we point out that the $\rho(\mathbf{p})$ reconstructed from the present set of 12 directions is not sensitive to the aforementioned bulge, suggesting that a set of directions clustered better around the [110] direction is necessary for delineating the presence or absence of this rather localized Fermi surface feature experimentally.

APPENDIX A

Here, we briefly describe how the value of $r_h = 23.1$ a.u. is obtained in connection with the filter function of Eq. (4.3). We write the function $h(x)$ obtained by convoluting a function $f(x)$ with a Gaussian $g(x) = e^{-(x/a)^2}$ as

$$h(x) = \int f(x-t)e^{-(t/a)^2}dt. \qquad (A1)$$

The Fourier transform of $h(x)$ is

$$\int h(x)e^{-irx}dx = \pi\sqrt{a}e^{-(ar/2)^2}\int f(x)e^{-irx}dx = G(r)F(r). \qquad (A2)$$

Here $G(r)$ and $F(r)$ are the Fourier transforms of $g(x)$ and $f(x)$, respectively, and the second equation represents the
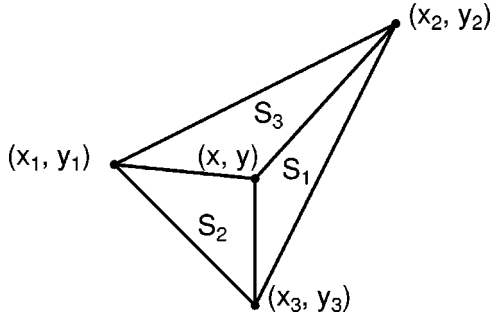
FIG. 9. Linear interpolation between three points.

standard ''Faltung'' theorem of Fourier transform. An important relationship can be obtained between a resolution function and its Fourier transform. Let $g(x_h) = 1/2$ and $G(r_h)/G(0) = 1/2$; then

$$x_h r_h = 2 \ln 2. \tag{A3}$$

For the experimental CP's, we assume that the resolution function is expressed by a Gaussian $(1/2)^{(p/x_h)^2}$, with $x_h = 0.06$ a.u. From Eq. (A3), this resolution function in the reciprocal space corresponds to a Gaussian $(1/2)^{(r/r_h)^2}$ with the value of $r_h = 23.1$ a.u.

APPENDIX B

We briefly discuss the three-point interpolation formula [Eq. (4.4)] and comment on a few related subtleties. First assume a linear function f given at three points (x_1, y_1, z_1), (x_2, y_2, z_2), and (x_3, y_3, z_3), where the z_i coordinate denotes the function value f_i at point (x_i, y_i) (cf. Fig. 9). A point (x, y) is situated within the triangle defined by these three points; z denotes the interpolated value f_z being sought. The plane through the three points in question may be defined by

$$a(x - x_1) + b(y - y_1) + c(f_z - f_1) = 0,$$

$$a(x - x_2) + b(y - y_2) + c(f_z - f_2) = 0, \tag{B1}$$

$$a(x - x_3) + b(y - y_3) + c(f_z - f_3) = 0.$$

This set of equations has a nonzero solution a, b, c only if its determinant is zero. Splitting up the determinant yields

$$\begin{vmatrix} x - x_1 & y - y_1 & f_z \\ x - x_2 & y - y_2 & f_z \\ x - x_3 & y - y_3 & f_z \end{vmatrix} - \begin{vmatrix} x - x_1 & y - y_1 & f_1 \\ x - x_2 & y - y_2 & f_2 \\ x - x_3 & y - y_3 & f_3 \end{vmatrix} = 0. \tag{B2}$$

Using the rule for addition of determinants several times, and noting that the area S of the triangle defined by the points (x_1, y_1), (x_2, y_2), and (x_3, y_3) is given by[59]

$$S = \frac{1}{2} \begin{vmatrix} x_1 & y_1 & 1 \\ x_2 & y_2 & 1 \\ x_3 & y_3 & 1 \end{vmatrix}, \tag{B3}$$

the first determinant in Eq. (B2) can be reduced to $2f_z S$. Similarly, the area S_1 of the subtriangle defined by the points (x, y), (x_2, y_2), and (x_3, y_3) can be written as

$$S_1 = \frac{1}{2} \begin{vmatrix} x & y & 1 \\ x_2 & y_2 & 1 \\ x_3 & y_3 & 1 \end{vmatrix}$$

$$= \frac{1}{2}(x_2 y_3 - x_3 y_2 - xy_3 + x_3 y + xy_2 - x_2 y). \tag{B4}$$

By inspection it is clear that the expression within brackets on the right-hand side of Eq. (B4) is equal to the cofactor of f_1 in the second determinant in Eq. (B2). Thus it has been shown that

$$f_z = (f_1 S_1 + f_2 S_2 + f_3 S_3)/S, \tag{B5}$$

i.e., the weights in the interpolation are found from the areas of the subtriangles opposite the respective points. In our case, the four points (i.e., the point where the interpolated value is sought and the three other points) will usually not lie in a plane, although deviations will in general be small; however, since any four points define the surface of a unique sphere, we can approximately map our problem to one of interpolating a linear function of solid angles on the surface of a sphere. It is resonable thus to use formula (B5) with the planar areas of various triangles replaced by the corresponding spherical areas. Strictly, of course, one needs independent function values at four noncoplanar points for a general three-dimensional linear interpolation problem.

Although the method described above has been used to obtain the coefficients u_i in Eq. (4.4), we note that the crystal symmetry will be more naturally accounted for by expanding $B(\mathbf{r})$ into normalized lattice harmonics (in the present case the Kubic harmonics of Von der Lage and Bethe[60])

$$B_i(\mathbf{r}) = \sum_l b_l(r) K_l(\Omega_i), \tag{B6}$$

where $K_l(\Omega_i)$ is the lattice harmonic of order l, and Ω_i denotes the ith direction. By solution of this set of equations, $b_l(r)$ can be expressed as linear combinations of the B_i as follows:

$$b_l(r) = \sum_k c_{kl} B_k(\mathbf{r}). \tag{B7}$$

The interpolated value $B(j_x, j_y, j_z)$ for the direction (j_x, j_y, j_z) is then found from

$$B(j_x, j_y, j_z) = \sum_l b_l(r) K_l(j_x, j_y, j_z) = \sum_k v_k B_k(\mathbf{r}), \tag{B8}$$

where, using Eq. (B7), $v_k = \Sigma_l c_{kl} K_l(j_x, j_y, j_z)$. Although formula (B8) better accounts for crystal symmetry, it may be more susceptible to noise than the linearized method of Eq. (B5).

APPENDIX C

Here we derive an approximate expression for the difference between the true value of the Fermi-surface radius and that given by the position of the maximum in the radial derivative, i.e., the inflection point in $\rho(p)$ where the second derivative rapidly changes sign. This analysis is used to make the corrections to radii invoked in connection with Figs. 7 and 8. Consider a model consisting of a free-electron Fermi sphere of radius p_f within which the momentum density $\rho(p)$ is unity:

$$\rho(p) = \begin{cases} 1 & \text{if} \quad p \leq p_f \\ 0 & \text{if} \quad p > p_f. \end{cases} \tag{C1}$$

The CP for this momentum distribution is

$$J(p_z) = \begin{cases} \pi(p_f^2 - p_z^2) & \text{if} \quad p_z \leq p_f \\ 0 & \text{if} \quad p_z > p_f. \end{cases} \tag{C2}$$

Let us assume that the profile is measured with a Gaussian resolution given by $R(p) = (1/\lambda \sqrt{\pi}) \exp(-p^2/\lambda^2)$, i.e., the FWHM of $R(p)$ is $2\lambda(\ln 2)^{1/2}$. The measured CP, J_m, is then given by

$$J_m(p_z) = (\pi^{1/2}/\lambda) \int_{-p_f}^{p_f} (p_f^2 - p^2) \exp[-(p - p_z)^2/\lambda^2] dp$$

$$= \pi^{1/2} \left[p_f^2 \int_{a_z}^{b_z} \exp(-u^2) du - \int_{a_z}^{b_z} (\lambda u + p_z)^2 \right.$$

$$\left. \times \exp(-u^2) du \right], \tag{C3}$$

where $a_z = (-p_f - p_z)/\lambda$ and $b_z = (p_f - p_z)/\lambda$. Since the momentum distribution is isotropic,

$$\rho(p) = -(2\pi p)^{-1} dJ_m(p)/dp$$

$$= \pi^{-1/2} \left\{ \int_a^b \exp(-u^2) du - \lambda/2p \right.$$

$$\left. \times [\exp(-b^2) - \exp(-a^2)] \right\}, \tag{C4}$$

with $a = (-p_f - p)/\lambda$ and $b = (p_f - p)/\lambda$. The second and third terms in Eq. (C4) are vanishingly small except in the vicinity of $\pm p_f$. From Eq. (C4), it follows that

$$d\rho(p)/dp = \pi^{-1/2}\{\lambda/2p^2[\exp(-b^2) - \exp(-a^2)] - (p_f/p)$$

$$\times [\exp(-b^2) + \exp(-a^2)]\} \tag{C5}$$

and

$$d^2\rho(p)/dp^2 = \pi^{-1/2} \left\{ \left[\frac{2p_f}{\lambda^3}\left(1 - \frac{p_f}{p}\right) + \frac{1}{\lambda p}\left(\frac{2p_f}{p} - 1\right) - \frac{\lambda}{p^3} \right] \right.$$

$$\times \exp(-b^2) + \left[\frac{2p_f}{\lambda^3}\left(1 + \frac{p_f}{p}\right) + \frac{1}{\lambda p}\left(\frac{2p_f}{p} + 1\right) \right.$$

$$\left. + \frac{\lambda}{p^3} \right] \exp(-a^2) \right\}. \tag{C6}$$

Concentrating on the region $p \sim +p_f$, we set $p = p_f + \delta$, and note that $\exp(-a^2) \sim 0$, while δ and λ are both much smaller than the Fermi radius p_f. The position of the inflection point of $\rho(p)$ is found by requiring that $d^2\rho(p)/dp^2 = 0$. Keeping only the lowest powers of δ/λ and λ/p_f, one finds

$$\delta \sim -\lambda^2/2p_f. \tag{C7}$$

Thus the use of the inflection point *underestimates* the Fermi radius. This systematic error increases quadratically with the FWHM of the resolution, which stresses the importance of a high resolution.

The quadratic addition of the extra resolution of 0.03-a.u. FWHM (i.e., $\lambda = 0.018$ a.u. and $\delta = -0.0003$ a.u.), caused by the reconstruction process (without filtering) of *unconvoluted* curves, and the optical resolution of the experiment (0.12-a.u. FWHM) yields a total resolution of 0.124-a.u. FWHM (i.e., $\lambda = 0.074$ a.u.) and $\delta = -0.0046$ a.u., i.e., the Fermi radius estimated from the position of the inflection point is 0.8% too small. If the reconstruction is performed on a set of *unconvoluted* curves but with filtering, the total resolution is 0.07-a.u. FWHM, which yields $\delta = -0.0015$ a.u., i.e., 0.25%. Finally, the combined resolution from convolution, reconstruction, and filtering is 0.139-a.u. FWHM, so $\delta = -0.0058$ a.u., resulting in a radius that is *underestimated* by 1%.

Incidentally, another method often used to estimate the Fermi radius consists of finding the position of the maximum in the second derivative of a profile, i.e., the zero of $d^3 J(p)/dp^3$. A similar analysis as given above shows that that method *overestimates* the Fermi radius by the amount $\delta \sim \lambda^2/2p_f$.

[1] A. Bansil, Z. Naturforsch. Teil A **48a**, 165 (1993).

[2] P. E. Mijnarends and A. Bansil, in *Positron Spectroscopy of Solids*, edited by A. Dupasquier and A. P. Mills, Jr. (IOS, Amsterdam, 1995), p. 25.

[3] S. Manninen, J. Phys. Chem. Solids **61**, 335 (2000).

[4] Y. Sakurai, Y. Tanaka, A. Bansil, S. Kaprzyk, A. T. Stewart, Y. Nagashima, T. Hyodo, S. Nanao, H. Kawata, and N. Shiotani, Phys. Rev. Lett. **74**, 2252 (1995).

[5] W. Schülke, G. Stutz, F. Wohlert, and A. Kaprolat, Phys. Rev. B **54**, 14 381 (1996).

[6] K. Hämäläinen, S. Manninen, C.-C. Kao, W. Caliebe, J. B. Hastings, A. Bansil, S. Kaprzyk, and P. M. Platzman, Phys. Rev. B **54**, 5453 (1996).

[7] M. Itou, Y. Sakurai, T. Ohata, A. Bansil, S. Kaprzyk, Y. Tanaka, H. Kawata, and N. Shiotani, J. Phys. Chem. Solids **59**, 99 (1998).

[8] S. Huotari, K. Hämäläinen, S. Manninen, S. Kaprzyk, A. Bansil, W. Caliebe, T. Buslaps, V. Honkimäki, and P. Suortti, Phys. Rev. B **62**, 7956 (2000).

[9] N. Shiotani, Y. Tanaka, Y. Sakurai, N. Sakai, M. Ito, F. Itoh, T. Iwazumi, and H. Kawata, J. Phys. Soc. Jpn. **62**, 239 (1993).

[10] Y. Sakurai, S. Kaprzyk, A. Bansil, Y. Tanaka, G. Stutz, H. Kawata, and N. Shiotani, J. Phys. Chem. Solids **60**, 905 (1999).

[11] G. Stutz, F. Wohlert, A. Kaprolat, W. Schülke, Y. Sakurai, Y. Tanaka, M. Ito, H. Kawata, N. Shiotani, S. Kaprzyk, and A. Bansil, Phys. Rev. B **60**, 7099 (1999).

[12] P. Suortti, T. Buslaps, V. Honkimäki, C. Metz, A. Shukla, Th. Tschentscher, J. Kwiatkowska, F. Maniawski, A. Bansil, S. Kaprzyk, A. S. Kheifets, D. R. Lun, T. Sattler, J. R. Schneider, and F. Bell, J. Phys. Chem. Solids **61**, 397 (2000).

[13] I. Matsumoto, J. Kwiatkowska, F. Maniawski, A. Bansil, S. Kaprzyk, M. Itou, H. Kawata, and N. Shiotani, J. Phys. Chem. Solids **61**, 375 (2000).

[14] See, e.g., M. J. Cooper, Rep. Prog. Phys. **48**, 415 (1985).

[15] The positron annihilation experiment of course measures the momentum density of the electron-positron pair.

[16] P. E. Mijnarends, Phys. Rev. **160**, 512 (1967); **178**, 622 (1969).

[17] P. E. Mijnarends, in *Compton Scattering*, edited by B. Williams (McGraw-Hill, New York, 1977), Ch. 10.

[18] A. M. Cormack, J. Appl. Phys. **34**, 2722 (1963); **35**, 2908 (1964).

[19] N. K. Hansen (unpublished).

[20] R. Suzuki, S. Tanigawa, N. Shiotani, M. Matsumoto, and S. Wakoh, in *Positron Annihilation*, edited by L. Dorikens-Vanpraet, M. Dorikens, and D. Segers (World Scientific, Singapore, 1989), p. 245.

[21] Y. Tanaka, N. Sakai, Y. Kubo, and H. Kawata, Phys. Rev. Lett. **70**, 1537 (1993).

[22] A variation of the direct Fourier method was used by Mueller (Ref. 23), who obtained the $B(\mathbf{r})$ distribution by interpolation between the measured profiles.

[23] F. M. Mueller, Phys. Rev. B **15**, 3039 (1977).

[24] G. Kontrym-Sznajd, R. N. West, and S. B. Dugdale, Mater. Sci. Forum **255-257**, 796 (1997).

[25] S. B. Dugdale, H. M. Fretwell, K. J. Chen, Y. Tanaka, A. Shukla, T. Buslaps, Ch. Bellin, G. Loupias, M. A. Alam, A. A. Manuel, P. Suortti, and N. Shiotani, J. Phys. Chem. Solids **61**, 361 (2000).

[26] L. Dobrzynski and A. Holas, Nucl. Instrum. Methods Phys. Res. A **383**, 589 (1996).

[27] H. G. Smith, Phys. Rev. Lett. **58**, 1228 (1987).

[28] M. B. Hunt, P. H. P. Reinders, and M. Springford, J. Phys. Chem. **1**, 6589 (1989).

[29] E. Daniel and S. H. Vosko, Phys. Rev. **120**, 2041 (1960).

[30] B. I. Lundqvist, Phys. Kondens. Mater. **6**, 206 (1967).

[31] A. W. Overhauser, Phys. Rev. B **3**, 1888 (1971).

[32] L. J. Lantto, Phys. Rev. B **22**, 1380 (1980).

[33] B. Farid, B. Heine, G. Engel, and I. Robertson, Phys. Rev. B **48**, 11 602 (1993).

[34] B. Holm and U. von Barth, Phys. Rev. B **57**, 2108 (1998).

[35] B. Kralik, P. Delaney, and S. G. Louie, Phys. Rev. Lett. **80**, 4253 (1998).

[36] C. Filippi and D. M. Ceperley, Phys. Rev. B **59**, 7907 (1999).

[37] B. Barbiellini, J. Phys. Chem. Solids **61**, 341 (2000).

[38] A. G. Eguiluz, W. Ku, and J. M. Sullivan, J. Phys. Chem. Solids **61**, 383 (2000).

[39] Y. Kubo, J. Phys. Soc. Jpn. **65**, 16 (1996).

[40] Y. Sakurai, M. Ito, T. Urai, Y. Tanaka, N. Sakai, T. Iwazumi, H. Ando, and N. Shiotani, Rev. Sci. Instrum. **63**, 1190 (1992).

[41] H. Kawata, M. Sato, T. Iwazumi, M. Ando, N. Sakai, M. Ito, Y. Tanaka, N. Shiotani, F. Itoh, H. Sakurai, Y. Sakurai, Y. Watanabe, and S. Nanao, Rev. Sci. Instrum. **62**, 2109 (1991).

[42] Y. Amemiya, T. Matsubara, A. Nakagawa, Y. Sato, J. Miyahara, and J. Chikawa, Nucl. Instrum. Methods Phys. Res. A **266**, 645 (1988).

[43] N. Sakai, J. Phys. Soc. Jpn. **56**, 2477 (1987).

[44] M. Ito and Y. Amemiya, Nucl. Instrum. Methods Phys. Res. A **310**, 369 (1991).

[45] A. Bansil and S. Kaprzyk, Phys. Rev. B **43**, 10 335 (1991).

[46] S. Kaprzyk and A. Bansil, Phys. Rev. B **42**, 7358 (1990).

[47] A. Bansil, S. Kaprzyk, and J. Toboła, in *Applications of Multiple Scattering Theory to Materials Science*, edited by W. H. Bulter, P. M. Oederichs, A. Gonis, and R. Weaver, MRS Symposia Proceedings No. 253 (Materials Research Society, Pittsburgh, 1992), p. 505.

[48] A. Bansil, S. Kaprzyk, P. E. Mijnarends, and J. Toboła, Phys. Rev. B **60**, 13 396 (1999).

[49] Our band structure of Li is in good accord with various published results, e.g., that of V. L. Moruzzi *et al.* [*Calculated Electronic Properties of Metals* (Pergamon Press, New York, 1978)].

[50] L. Lam and P. M. Platzman, Phys. Rev. B **9**, 5122 (1974). Although the Lam-Platzman correction, included in the results presented here, reduces the discrepancy between theory and experiment, its overall effect is relatively small.

[51] R. J. Barlow, *Statistics* (Wiley, New York, 1989).

[52] N. K. Hansen, P. Pattison, and J. R. Schneider, Z. Phys. B: Condens. Matter **66**, 305 (1987).

[53] Notably, temperature effects (lattice expansion, Debye-Waller factor) are expected to reduce the high momentum components (Ref. 54).

[54] C. Sternemann, G. Döring, C. Wittkop, W. Schülke, A. Shukla, T. Buslaps, and P. Suortti, J. Phys. Chem. Solids **61**, 379 (2000).

[55] However, as discussed in Appendix C, a correction of 0.25% should be applied to account for the effect of filtered reconstruction which yields a reconstructed radius of 0.5793 a.u. compared to the original value of 0.5764 a.u.

[56] L. Oberli, A. A. Manuel, R. Sachot, P. Descouts, and M. Peter, Phys. Rev. B **31**, 6104 (1985).

[57] We note in this connection that Schülke *et al.* (Ref. 5) and Oberli *et al.* (Ref. 56) each used different procedures to analyze their data in Li. Schülke *et al.* (Ref. 5) obtained the occupation density from their reconstructed momentum density and find the contour with a constant occupancy of 0.5 to define the Fermi surface reasonably. Oberli *et al.* (Ref. 56), on the other hand, determine the Fermi radius with respect to the slope from model studies which indicate that the radius can be defined reliably at

84% of the derivative peak. The data of Schülke *et al.* (Ref. 5) and Oberli *et al.* (Ref. 56) therefore do not require any further correction.

[58] The reconstruction of the unconvoluted theoretical profiles shown in Fig. 3 yields a [110] radius of 0.597 a.u. with filtering (cf. the dotted curve in Fig. 7) and 0.604 a.u. without filtering (not shown). After correction these values become 0.599 and 0.604 a.u., respectively.

[59] J. W. Harris and H. Stocker, *Handbook of Mathematics and Computational Science* (Springer, New York, 1998), p. 378.

[60] F. C. Von der Lage and H. A. Bethe, Phys. Rev. **71**, 612 (1947).